Hindawi
Complexity
Volume 2022, Article ID 3505634, 14 pages
https://doi.org/10.1155/2022/3505634

WILEY | Hindawi

Research Article

Existence of Solution and Self-Exciting Attractor in the Fractional-Order Gyrostat Dynamical System

Muhammad Marwan,[1] **Gauhar Ali**,[2] **and Ramla Khan**[3]

[1]*College of Mathematics and Computer Science, Zhejiang Normal University, Jinhua, Zhejiang 321004, China*
[2]*Department of Mathematics, University of Malakand, Malakand, Pakistan*
[3]*School of Environment Earth and Ecosystem Sciences (EEES) School, The Open University, Milton Keynes MK76AA, UK*

Correspondence should be addressed to Gauhar Ali; gauharali4@gmail.com

Received 25 March 2022; Revised 5 May 2022; Accepted 9 May 2022; Published 18 July 2022

Academic Editor: Chun-Biao Li

This work identifies the influence of chaos theory on fractional calculus by providing a theorem for the existence and stability of solution in fractional-order gyrostat model with the help of a fixed-point theorem. We modified an integer order gyrostat model consisting of three rotors into fractional order by attaching rotatory fuel-filled tank and provided an iterative scheme for our proposed model as a working rule of obtained analytical results. Moreover, this iterative scheme is injected into algorithms for a system of integer order dynamical systems to observe Lyapunov exponents and a bifurcation diagram for our proposed fractional-order dynamical model. Furthermore, we obtained five equilibrium points, including four unstable spirals and one saddle node, using local dynamical analysis which acted as self-exciting attractors and a separatrix in a global domain.

1. Introduction

System of ordinary differential equations [1]

$$\dot{x} = f(x, \beta). \tag{1}$$

Is called the dynamical system, and a parameter $\beta \in \mathbb{R}$ in the velocity vector field is termed as bifurcation parameter if system (1) changes its topological structure with the variation in parameter values, whereas the process of changing in qualitative structures is known as bifurcation. There are several types of bifurcation including saddle node [2], Hopf [3–7], and zero-Hopf [8–11]. The bifurcation diagram [12] for the parameter makes it easy for predicting the type of bifurcation and existence of chaos in system (1). Chaos has a vital role in engineering [13–17], medical [18–20], aeronautics [14, 21] and fluid dynamics [22–24]. Apart from the above cited applications, its great influence can also be found in fractional calculus [25–27] and reference therein. Dynamical systems based on ordinary differential equations with an integer order, $\gamma = 1$, describe velocity vectors, but for fractional order, $\gamma \in (0, 1)$, researchers aim to target velocity vectors and replace it by differential equation with order between 0 and 1. Several discretization techniques such as fractional linear multistep [28], Adam [29], predictor-corrector [30], and Adam–Bashforth/Moulton [31] are used to solve fractional-order dynamical systems since decade, but the most flexible scheme with fast convergence in solving nonlinear problems is the variation iteration method (VIM). This technique was used for integer order dynamical systems, but later on modified for fractional-order systems by introducing Lagrangian multiplier [32] into it. Many researchers have enhanced its importance by using it in several engineering-based complex problems, such as in 2006, the variation iteration scheme was utilized for fractional-order systems by Odibat and Momani [33], whereas new development in the VIM was carried by Wu and Baleanu [32] in 2013 to overcome its limitation. Recently in 2021, Kumar and Gupta [34] worked on application of the VIM in a fuzzy-based system.

It has been observed from the above-cited work and our knowledge from the literature that dynamical systems related to spacecrafts or its attached devices such as beam and gyrostat have never been considered for the existence of

solution and self-exciting attractors in a fractional-order form. Therefore, we have restructured the gyrostat chaotic system [35] into a fractional order along with the addition of a rotatory liquid-filled tank to discuss its unique solution, bounds, and stability using the fixed point theory. Moreover, for bringing novelty into our work, a variation iteration scheme has been used in our proposed fractional-order system to observe chaos into it. For this purpose, several algorithms such as by Wolf et al. [36] and the bifurcation diagram [37] were modified by injecting the VIM iteration scheme into these algorithms. Finally, analyzing local dynamics of our proposed model, trajectories around five equilibrium points with four unstable spirals and a single saddle node motivated us to search for self-exciting attractors with a separatrix in a global domain.

The following pattern can be followed for understanding the rest of the paper. In Section 2, the gyrostat chaotic system is remodeled by adding rotatory liquid-filled tank and modified into fractional order. Several theorems have been proved in Section 3 for the existence of solution and stability. An iteration scheme for our proposed model has been introduced in Section 4, while several applications of this scheme related to dynamical analysis are discussed in Section 5. Finally, Section 6 comprises concluding remarks and future target.

2. Modeling of Gyro Chaotic System Attached with Fuel-Filled Tank

Gyrostat is a device consisting of rotors, used as an attachment in larger objects for bringing stability in their dynamics with the passage of time. The system of three-dimensional ordinary differential equations for the gyrostat model is designed by Qi et al. [35]:

$$\begin{cases} I_x\dot{x} = \left(I_y - I_z\right)yz - yh_z + zh_y - T_x + L_x, \\ I_y\dot{y} = \left(I_z - I_x\right)zx - zh_x + xh_z - T_y + L_y, \\ I_z\dot{z} = \left(I_x - I_y\right)xy - xh_y + yh_x - T_z + L_z, \end{cases} \tag{2}$$

where $X = [xyz]^T$ is the angular velocity vector, $I = [I_x, I_y, I_z]$ are the principal moments of inertia of the gyrostat in the body axis frame, $H = [h_x, h_y, h_z]$ are constants of total angular momentum, whereas $L = [L_x, L_y, L_z]$ and $T = [T_x, T_y, T_z]$ are external and disturbed torques applied on the gyrostat, respectively.

A tank, rotating about an angle θ at desired point $(\overline{x}, \overline{y}, \overline{z})$ (shown in Figure 1), is attached with an originally disturbed gyrostat system given in (2). It is observed that $L = (L_x, L_y, L_z)$ is a vector of external forces applied on the gyrostat. Therefore, we have attached a tank containing fuel which exert external forces on the gyrostat due to rotation of the attached tank with respect to $z-$ axis about angle θ at desired point $(\overline{x}, \overline{y}, \overline{z})$. Hence, we replaced L with

$$R = R_z(\theta)\overline{d}(x), \tag{3}$$

where $R = (R_x, R_y, R_z)$, $R_z(\theta)$ is the rotation matrix for $z-$ axis and $\overline{d}(x)$ is a desired point about which one can rotate the attached tank. Therefore, using vector T in ((2) [38]) and R given in (3) into (2), we obtain the following equation:

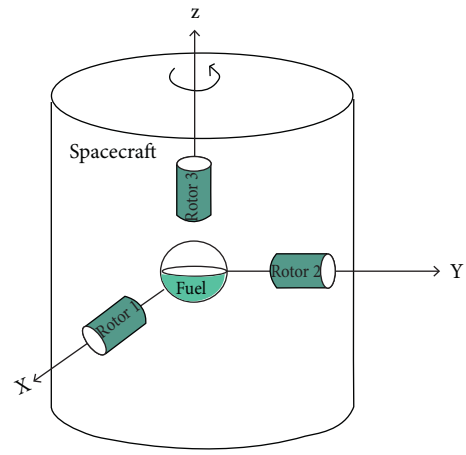

Figure 1: Spacecraft attached with partially filled fuel tank and three rotors. This figure is reproduced from the work of Sabir et al. [7] with the assumption that the third rotor is rotating about z-axis.

$$\begin{cases} I_x^C\mathscr{D}^\gamma x = \left(I_y - I_z\right)yz - yh_z + zh_y - \mu_x x + \overline{x}\cos(\theta) - \overline{y}\sin(\theta), \\ I_y^C\mathscr{D}^\gamma y = \left(I_z - I_x\right)zx + xh_z + \mu_y y + \overline{x}\sin(\theta) + \overline{y}\cos(\theta), \\ I_z^C\mathscr{D}^\gamma z = \left(I_x - I_y\right)xy - xh_y - \mu_z z + \overline{z}, \end{cases} \tag{4}$$

System (4) is a fractional-order mathematical representation of the model given in Figure 1 in which γ is the fractional number between 0 and 1 exclusive, $u = (u_x, u_y, u_z)$ is a damping constant vector, while X, I, and H are defined in equation (2). Moreover, system (4) shows chaotic behavior for $X = [0.1, 0.1, 0.1]$, $I = [0.85, 0.45, 0.2]$, $u = [6, 6.42, 5.8]$, $H = [0, 0.57416, 2, 38]$, and $R = [-20, 2, 20]$. The phase portrait of system (4) with given initial and parameter values can be seen in region 10 of Figure 2.

3. Existence and Stability of Solution

In this part of our paper, we determined results based on the existence theory for system (4) using the fixed point theorem with Banach space. Therefore, basic definitions and important lemmas are considered for the understanding of this work.

Definition 1 (see [39]). The integral of fractional order $\gamma 0$ for a function ϖ is given by

$$\mathscr{I}^\gamma\varpi(t) = \frac{1}{\Gamma(\gamma)}\int_0^t (t-\eta)^{\gamma-1}\varpi(\eta)d\eta\ . \tag{5}$$

Definition 2 (see [39]). The Caputo fractional derivative of order $\gamma 0$ of a continuous function ϖ is given by

$${}^C\mathscr{D}^\gamma\varpi(t) = \frac{1}{\Gamma(n-\gamma)}\int_0^t (t-\eta)^{n-\gamma-1}\varpi^{(n)}(\eta)d\eta\ , \tag{6}$$

where $n = [\gamma] + 1$.

Following two lemmas have importance in achieving the solutions of the systems consisting of fractional differential equations.

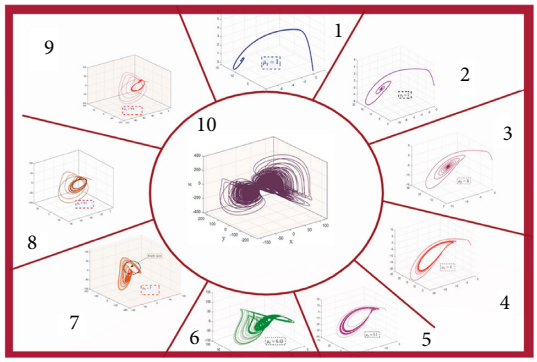

FIGURE 2: Existence of chaos in clockwise and anticlockwise directions.

Lemma 1 (see [39]). *Assume $\varpi \in C(0,1)$, then the solution of fractional differential equation*

$$^{C}\mathscr{D}^{\gamma}\varpi(t) = 0, \tag{7}$$

Of order $\gamma 0$ is

$$\varpi(t) = c_0 + c_1 t + \cdots + c_{n-1}t^{n-1}, \quad c_i \in \mathscr{R},\ i = 0, 2, \ldots, n-1. \tag{8}$$

Lemma 2 (see [39]). *Let us consider $\varpi \in C(0,1)$, with a derivative of fractional order γ, then*

$$\mathscr{I}^{\gamma\,C}\mathscr{D}^{\gamma}\varpi(t) = \varpi(t) + c_0 + c_1 t + \cdots + c_{n-1}t^{n-1}, \quad c_i \in \mathscr{R},\ i = 0, 2, \ldots, n-1. \tag{9}$$

We begin our work by introducing ϖ_1, ϖ_2, and ϖ_3 on the right side of equation (4) and for convenience, we use the following notions:

$$\chi(t) = \begin{cases} x(t), \\ y(t), \chi_0 = \\ z(t), \end{cases} \begin{cases} x(0), \\ y(0), \Psi(t, \chi(t)) = \\ z(0), \end{cases} \begin{cases} \varpi_1(t,x,y,z), \\ \varpi_2(t,x,y,z), \\ \varpi_3(t,x,y,z), \end{cases} \tag{10}$$

and

$$\Psi_0 = \begin{cases} \varpi_1(0, x(0), y(0), z(0)), \\ \varpi_2(0, x(0), y(0), z(0)), \\ \varpi_3(0, x(0), y(0), z(0)), \end{cases} \tag{11}$$

System (4) can be rewritten, using (5) as

$$\begin{aligned} {}^{C}D_t^{\gamma}[\chi(t)] &= \Psi(t, \chi(t)), t \in [0, \tau], \\ \chi(0) &= \chi_0. \end{aligned} \tag{12}$$

According to Lemma 2, problem (12) can be converted into an integral equation

$$\chi(t) = \chi_0 + \frac{1}{\Gamma(\gamma)}\int_0^t (t-\eta)^{\gamma-1}\Psi(\eta, \chi(\eta))d\eta\ . \tag{13}$$

Definition 3. Let us consider $X = C([0,\tau]$ a Banach space under the suitable norm

$$\|\chi\| = \sup_{t\in J}\{|\chi|: \chi \in X\}, \tag{14}$$

and the operator is defined as

$$\tau\chi(t) = \chi_0 + \frac{1}{\Gamma(\gamma)}\int_0^t (t-\eta)^{\gamma-1}\Psi(\eta, \chi(\eta))d\eta\ , \tag{15}$$

where $0 \le t \le \tau < \infty$ and $J = [0, \tau]$. Then, the following assumptions are true:

$[(A_1)]$ There exists a positive constant $_{\Psi} > 0$ such that

$$\left|\Psi(t, \chi(t)) - \Psi(t, \overline{\chi}(t))\right| \le {}_{\Psi}\left|\chi(t) - \overline{\chi}(t)\right|. \tag{16}$$

$[(A_2)]$ The following inequality holds for positive constants $M_{\Psi}, G_{\Psi} > 0$:

$$|\Psi(t, \chi(t))| \le M_{\Psi}|\chi| + G_{\Psi}. \tag{17}$$

Theorem 1. *Let us consider that $_{\Psi}\tau^{\gamma} < \Gamma(\gamma+1)$ and assumption (A_2) is satisfied. Then, there exists a unique solution of system (4) with the contraction of operator τ.*

Proof. Let $\chi, \overline{\chi} \in X$, then one has

$$\begin{aligned} \|\tau\chi - \tau\overline{\chi}\| &= \sup_{t\in J}\left|\chi_0 + \frac{1}{\Gamma(\gamma)}\int_0^t (t-\eta)^{\gamma-1}\Psi(\eta, \chi(\eta))d\eta\right. \\ &\quad \left. -\left(\chi_0 + \frac{1}{\Gamma(\gamma)}\int_0^t (t-\eta)^{\gamma-1}\Psi(\eta, \overline{\chi}(\eta))d\eta\right)\right| \\ &\le \frac{1}{\Gamma(\gamma)}\int_0^{\tau} (t-\eta)^{\gamma-1}|\Psi(\eta, \chi(\eta)) - \Psi(\eta, \overline{\chi}(\eta))|d\eta \\ &\le \frac{1}{\Gamma(\gamma)}\int_0^{\tau} (t-\eta)^{\gamma-1}d\eta\ {}_{\Psi}|\chi(\eta)) - \overline{\chi}(\eta)| \\ &\le \frac{{}_{\Psi}\tau^{\gamma}}{\Gamma(\gamma+1)}\|\chi - \overline{\chi}\|. \end{aligned} \tag{18}$$

This shows that τ is a contraction. Hence, our desired result is obtained, that system (4) has a unique solution. □

Theorem 2. *The integral equation (8) has at least one solution if $_{\Psi} < \mathbb{G}(\gamma)$ under the assumptions of A_1 and A_2.*

Proof. For existence of a solution for operator τ, it is enough to show that τ is completely continuous, and there exists an

element $\chi \in X$ such that $\chi = \delta\tau(\chi)$ for $\delta \in (0,1)$. Therefore, our proof will pass through three steps for achieving our desired results. □

Step 1. Let us consider a sequence $\chi_n \longrightarrow \chi$ in X and for each $t \in J$, we have

$$\begin{aligned}\|\tau\chi_n - \tau\chi\| &= \sup_{t\in J} |\chi_0 + \frac{1}{\Gamma(\gamma)}\int_0^t (t-\eta)^{\gamma-1}\Psi(\eta,\chi_n(\eta))d\eta \\ &\quad -\left(\chi_0 + \frac{1}{\Gamma(\gamma)}\int_0^t (t-\eta)^{\gamma-1}\Psi(\eta,\chi(\eta))d\eta\right)| \\ &\le \frac{1}{\Gamma(\gamma)}\int_0^\tau (t-\eta)^{\gamma-1}|\Psi(\eta,\chi_n(\eta)) - \Psi(\eta,\chi(\eta))|d\eta\ .\end{aligned} \tag{19}$$

Hence, $\tau\chi_n$ approaches $\tau\chi$ as time t tends to infinity

$$\|\tau\chi_n - \tau\chi\| \longrightarrow 0 as n \longrightarrow \infty. \tag{20}$$

Equation (20) identifies continuity of an operator τ.

Step 2. Let us consider a bounded set $B_r = \{\chi \in X: \|\chi\| \le r\}$, where r is a positive real number. Then, for any $\chi \in B_r$, we have

$$\begin{aligned}\|\tau\chi\| &= \sup_{t\in J}\left|\chi_0 + \frac{1}{\Gamma(\gamma)}\int_0^t (t-\eta)^{\gamma-1}\Psi(\eta,\chi(\eta))d\eta\right| \\ &\le \chi_0 + \frac{1}{\Gamma(\gamma)}\int_0^\tau (\tau-\eta)^{\gamma-1}|\Psi(\eta,\chi(\eta))|d\eta \\ &\le \chi_0 + \frac{M_\Psi|\chi| + G_\Psi}{\Gamma(\gamma)}\int_0^\tau (\tau-\eta)^{\gamma-1}d\eta \\ &\le \chi_0 + \frac{(M_\Psi r + G_\Psi)\tau^\gamma}{\Gamma(\gamma+1)} = l.\end{aligned} \tag{21}$$

Hence, τ maps a bounded set into a bounded set.

Step 3. The image of a bounded set under τ is equicontinuous in X.

Let $t_1 < t_2$ in J and $\chi \in B_r$, we have

$$\begin{aligned}|\tau\chi(t_2) - \tau\chi(t_1)| &= |\chi_0 + \frac{1}{\Gamma(\gamma)}\int_0^{t_2} (t_2-\eta)^{\gamma-1}\Psi(\eta,\chi(\eta))d\eta \\ &\quad -\left(\chi_0 + \frac{1}{\Gamma(\gamma)}\int_0^{t_1} (t_1-\eta)^{\gamma-1}\Psi(\eta,\chi(\eta))d\eta\right)| \\ &= |\frac{1}{\Gamma(\gamma)}\left(\int_0^{t_1} (t_2-\eta)^{\gamma-1}\Psi(\eta,\chi(\eta))d\eta\right. \\ &\quad \left. + \int_{t_1}^{t_2} (t_2-\eta)^{\gamma-1}\Psi(\eta,\chi(\eta))d\eta - \int_0^{t_1} (t_1-\eta)^{\gamma-1}\Psi(\eta,\chi(\eta))d\eta\right)| \\ &\le \frac{1}{\Gamma(\gamma)}\left(\int_0^{t_1} (t_2-\eta)^{\gamma-1} + (t_1-\eta)^{\gamma-1}\Psi(\eta,\chi(\eta))d\eta + \int_{t_1}^{t_2} (t_2-\eta)^{\gamma-1}\Psi(\eta,\chi(\eta))d\eta\right. \\ &\le \frac{M_\Psi r + G_\Psi}{\Gamma(\gamma+1)}\left\{\int_0^{t_2} (t_2-\eta)^{\gamma-1}d\eta - \int_0^{t_1} (t_1-\eta)^{\gamma-1}d\eta\right\} \le \frac{M_\Psi r + G_\Psi}{\Gamma(\gamma+1)}\{t_2^\gamma - t_1^\gamma\}.\end{aligned} \tag{22}$$

As $t_2 \longrightarrow t_1$, then $|\tau\chi(t_2) - \tau\chi(t_1)| \longrightarrow 0$, and thus, τ is continuous and bounded. Hence, $\|\tau\chi(t_2) - \tau\chi(t_1)\| \longrightarrow 0$ shows uniform continuity of τ. Therefore, steps 1 – 3 show that τ is completely continuous.

Step 4. Finally, we have to show that $\mathscr{B} = \{\chi \in X: \chi = \delta\tau(\chi)\}$ for some $\delta \in [0,1]$, is bounded. Let $\chi \in \mathscr{B}$ and for any t, we have

$$\begin{aligned}\|\chi\| &= \sup_{t\in J} |\delta T(\chi)| \\ &= \sup_{t\in J} |\delta\chi_0 + \frac{\delta}{\Gamma(\gamma)}\int_0^t (t-\eta)^{\gamma-1}\Psi(\eta,\chi(\eta))d\eta| \\ &\le \chi_0 + \frac{1}{\Gamma(\gamma)}\int_0^\tau (\tau-\eta)^{\gamma-1}|\Psi(\eta,\chi(\eta))|d\eta\ , as \delta \le 1, \\ &\le \chi_0 + \frac{M_\Psi|\chi| + G_\Psi}{\Gamma(\gamma)}\int_0^\tau (\tau-\eta)^{\gamma-1}d\eta\ , \\ \|\chi\| &\le \chi_0 + \frac{(M_\Psi\|\chi\| + G_\Psi)\tau^\gamma}{\Gamma(\gamma+1)}.\end{aligned} \tag{23}$$

Simplifying inequality (19) yields

$$\|\chi\| \leq \frac{\chi_0 \Gamma(\gamma+1) + G_\Psi \tau^\gamma}{\Gamma(\gamma+1) - M_\Psi \tau^\gamma}. \tag{24}$$

This shows that the defined set $\mathscr{B}$ is bounded. Hence using Schaefer's theorem [40], system (4) has at least one solution.

For achieving stability, a negligible perturbation parameter $\theta(t)$ can be included in ${}_0^{CF}D_t^\gamma \chi(t)$ such that

(i) ${}_0^{CF}D_t^\gamma \chi(t) = \Psi(t, \chi(t)) + \theta(t)$
(ii) $|\theta(t)| < \varepsilon$ for $\varepsilon 0$

Lemma 3. *Solution of the perturbed problem*

$${}_0^{CF}D_t^\gamma \chi(t) = \Psi(t, \chi(t)) + \theta(t) \chi(0) = \chi_0, \tag{25}$$

Satisfies the following relation:

$$\left| \chi(t) - \left(\chi_0 + \left[\Psi(t, \chi(t)) - \Psi_0 \right] \frac{(1-\gamma)}{\mathbb{G}(\gamma)} + \frac{\gamma}{\mathbb{G}(\gamma)} \int_0^t \Psi(\eta, \chi(\eta)) d\eta \right) \right| \leq L_\Psi \varepsilon. \tag{26}$$

Theorem 3. *Gyrostat system (4) achieves Ullam–Hyers stability if $L_\Psi < 1$ and assumption A_2, together with Lemma 3 is satisfied.*

Proof. Let $\chi \in X$ be any solution and $\overline{\chi} \in X$ is a unique solution, then

$$\begin{aligned} |\chi(t) - \overline{(Y)}(t)| &= \left| \chi(t) - \left(\chi_0 + \left[\Psi(t, \overline{\chi}(t)) - \Psi_0 \right] \frac{(1-\gamma)}{\mathbb{G}(\gamma)} + \frac{\gamma}{\mathbb{G}(\gamma)} \int_0^t \Psi(\eta, \overline{\chi}(\eta)) d\eta \right) \right| \\ &\leq \left| \chi(t) - \left(\chi_0 + \left[\Psi(t, \chi(t)) - \Psi_0 \right] \frac{(1-\gamma)}{\mathbb{G}(\gamma)} + \frac{\gamma}{\mathbb{G}(\gamma)} \int_0^t \Psi(\eta, \chi(\eta)) d\eta \right) \right| \\ &\quad + \left| \left(\chi_0 + \left[\Psi(t, \chi(t)) - \Psi_0 \right] \frac{(1-\gamma)}{\mathbb{G}(\gamma)} + \frac{\gamma}{\mathbb{G}(\gamma)} \int_0^t \Psi(\eta, \chi(\eta)) d\eta \right) \right. \\ &\quad \left. - \left(\chi_0 + \left[\Psi(t, \overline{\chi}(t)) - \Psi_0 \right] \frac{(1-\gamma)}{\mathbb{G}(\gamma)} + \frac{\gamma}{\mathbb{G}(\gamma)} \int_0^t \Psi(\eta, \overline{\chi}(\eta)) d\eta \right) \right| \\ &\leq L_\Psi \varepsilon + L_\Psi \|\chi - \overline{\chi}\|. \end{aligned} \tag{27}$$

This implies that

$$\|\chi - \overline{\chi}\| \leq \frac{L_\Psi}{1 - L_\Psi} \varepsilon. \tag{28}$$

Hence, solution of the proposed system (4) is Ullam–Hyers stable. □

4. Variational Iterative Scheme for System (4)

An iterative scheme, variational iterative method (VIM), is introduced in this section using successive approximations of the solution for rapid convergence and analytical results discussed in Section 2.

4.1. Working Rule. To express the VIM, we consider general nonlinear differential equation as

$$\mathscr{L}\chi(t) + \mathscr{N}\chi(t) = h(t), \tag{29}$$

where $\mathscr{L}$, $\mathscr{N}$, and h are linear, nonlinear, and source functions, while the corrector function for (29) is considered as

$$\chi_{n+1}(t) = \chi_n(t) + \int_0^t \Lambda(\eta) \left(\mathscr{L}\chi(\eta) + \widetilde{\mathscr{N}}\chi(\eta) - h(\eta) \right) d\eta \,. \tag{30}$$

Λ in (30) is defined as $(-1)^n (t-\eta)^{n-1} / \Gamma(n)$, whereas $\widetilde{\mathscr{N}}$ is used as a restricted value with $\sigma\mathscr{N} = 0$. Then, the exact solution can be obtained as

$$\chi(t) = \lim_{n \longrightarrow \infty} \chi_n(t). \tag{31}$$

System (4) can be discretized using VIM as

$$\begin{aligned} x_{n+1} &= x_n - \mathcal{F}^{\gamma}\left(I_x^C\mathcal{D}^{\gamma}x_n - \left(I_y - I_z\right)y_n z_n + y_n h_z - z_n h_y + \mu_x x_n - \overline{x}\cos(\theta) + \overline{y}\sin(\theta)\right),\\ y_{n+1} &= y_n - \mathcal{F}^{\gamma}\left(I_y^C\mathcal{D}^{\gamma}y_n - (I_z - I_x)z_n x_n - x_n h_z - \mu_y y_n - \overline{x}\sin(\theta) - \overline{y}\cos(\theta)\right),\\ z_{n+1} &= z_n - \mathcal{F}^{\gamma}\left(I_z^C\mathcal{D}^{\gamma}z - \left(I_x - I_y\right)x_n y_n + x_n h_y + \mu_z z_n + \overline{z}\right), \end{aligned} \tag{32}$$

where $x(0) = x_0$, $y(0) = y_0$, and $z(0) = z_0$.

For $n = 0, 1$

$$\begin{cases} x_1 = x_0 + \dfrac{x^{\gamma}\kappa_{x1}}{\Gamma(\gamma+1)}, \\ y_1 = y_0 + \dfrac{y^{\gamma}\kappa_{y1}}{\Gamma(\gamma+1)}, \\ z_1 = z_0 + \dfrac{z^{\gamma}\kappa_{z1}}{\Gamma(\gamma+1)}, \end{cases} \begin{cases} x_2 = x_0 + \dfrac{\kappa_{x2}}{\Gamma(\gamma+1)}x^{\gamma} - \dfrac{\mu_x\kappa_{x1}}{\Gamma(2\gamma+1)}x^{2\gamma}, \\ y_2 = y_0 + \dfrac{\kappa_{y2}}{\Gamma(\gamma+1)}y^{\gamma} + \dfrac{\kappa_{y1}}{\Gamma(2\gamma+1)}y^{2\gamma}, \\ z_2 = z_0 + \dfrac{\kappa_{z2}}{\Gamma(\gamma+1)}z^{\gamma} - \dfrac{\left(\mu_z - h_y\right)\kappa_{z1}}{\Gamma(2\gamma+1)}z^{2\gamma}, \end{cases} \tag{33}$$

where

$$\begin{cases} \kappa_{x1} = -\left(I_y - I_z\right)y_0 z_0 + y_0 h_z - z_0 h_y + \mu_x x_0 - \overline{x}\cos(\theta) + \overline{y}\sin(\theta), \\ \kappa_{x2} = \kappa_{x1}(1 + I_x) - \left(I_y - I_z\right)y_1 z_1 + y_1 h_z - z_1 h_y + \mu_x x_0 - \overline{x}\cos(\theta) + \overline{y}\sin(\theta), \\ \kappa_{y1} = -(I_z - I_x)z_0 x_0 - x_0 h_z - \mu_y y_0 - \overline{x}\sin(\theta) - \overline{y}\cos(\theta), \\ \kappa_{y2} = L_y\left(1 + I_y\right) - (I_z - I_x)z_1 x_1 - x_1 h_z - \mu_y y_0 - \overline{x}\sin(\theta) - \overline{y}\cos(\theta), \\ \kappa_{z1} = -\left(I_x - I_y\right)x_0 y_0 + x_0 h_y + \mu_z z_0 - \overline{z}, \\ \kappa_{z2} = L_z(1 + I_z) - \left(I_x - I_y\right)x_1 y_1 + x_1 h_y + \mu_z z_1 - \overline{z}. \end{cases} \tag{34}$$

For $n = 2$, we have

$$\begin{cases} x_3 = x_0 + \dfrac{\rho 1/x}{\Gamma(\gamma+1)}x^{\gamma} - \dfrac{\rho 2/x}{\Gamma(2\gamma+1)}x^{2\gamma} + \dfrac{\rho 3/x}{\Gamma(3\gamma+1)}x^{3\gamma}, \\ y_3 = y_0 + \dfrac{1/y}{\Gamma(\gamma+1)}y^{\gamma} + \dfrac{2/y}{\Gamma(2\gamma+1)}y^{2\gamma} + \dfrac{3/y}{\Gamma(3\gamma+1)}y^{3\gamma}, \\ z_3 = z_0 + \dfrac{\varsigma 1/z}{\Gamma(\gamma+1)}z^{\gamma} - \dfrac{\varsigma 2/z}{\Gamma(2\gamma+1)}z^{2\gamma} + \dfrac{\varsigma 3/z}{\Gamma(3\gamma+1)}z^{3\gamma}. \end{cases} \tag{35}$$

The values of ρ_x^i, ϱ_y^i and ς_z^i, $i = 1, 2, 3$ in (35) are given in Appendix *A*. In the next section, we have discussed system (4) analytically and qualitatively. For numerical simulations, our designed algorithm is used to plot Lyapunov exponents and bifurcation diagram in integer order as well as fractional-order chaotic systems.

5. Dynamical Analysis

The fractional-order dynamical system exhibits chaos for some values of fractional term, γ, but using a hit and trial method for such purpose is difficult to investigate chaos in dynamical systems. Therefore, we plotted the bifurcation diagram for

system (4) with respect to fractional term, γ. A noisy dense area is observed in Figure 3 that illustrates occurrence of chaos in the fractional-order gyrostat system beginning with $\gamma = 0.86$.

In section 2, we used the concept of the fixed point theory to obtain at least one solution of system (4). Hence, for fixed points, we consider the following function ϖ_i, $i = 1, 2, 3$ equals to zero:

$$\begin{cases} \varpi_1 = \left(I_y - I_z\right)yz - yh_z + zh_y - \mu_x x + \overline{x}\cos(\theta) - \overline{y}\sin(\theta) = 0, \\ \varpi_2 = \left(I_z - I_x\right)zx + xh_z + \mu_y y + \overline{x}\sin(\theta) + \overline{y}\cos(\theta) = 0, \\ \varpi_3 = \left(I_x - I_y\right)xy - xh_y - \mu_z z + \overline{z} = 0. \end{cases} \tag{36}$$

After fixing all parameters given in section (1), then we solve equation (36) to get the following five equilibrium points:

$$\begin{cases} E_1 = [-0.819, 3.141, 3.352]^T, \\ E_2 = [-11.078, 14.8464, -6.79773]^T, \\ E_3 = [12.445, -15.8945, -11.4255]^T, \\ E_4 = [11.5523, 22.4277, 20.1731]^T, \\ E_5 = [-12.4328, -23.1278, 24.5096]^T. \end{cases} \tag{37}$$

In Theorem 4 local dynamical analysis of system (4) is used for observing trajectories around equilibrium points (27).

Theorem 4. *A gyrostat chaotic system (4) is composed of five equilibrium points, in which E_1 is the saddle node and $E_{2,3,4,5}$ are all unstable saddle spirals. Moreover, these spirals lead to four attractors and one saddle node E_1 that act as a separatrix as t extends.*

Proof. Five equilibrium points are calculated in equation (27). The Jacobian matrix plays a vital role in the system of differential equations for local dynamical analysis. Therefore, the Jacobian matrix of system (4) is

$$J = \begin{pmatrix} \frac{-120}{17} & \frac{5z}{17} - \frac{14}{5} & \frac{5y}{17} + \frac{7177}{10625} \\ \frac{238}{45} - \frac{(13z)}{9} & \frac{214}{15} & -\frac{(13x)}{9} \\ 2y - \frac{7177}{2500} & 2x & -29 \end{pmatrix}. \tag{38}$$

And the Jacobian matrix for fixed parameter values at E_1 is

$$J|_{E_1} = \begin{pmatrix} -7.0588 & -1.8142 & 1.5993 \\ 0.4473 & 14.2667 & 1.1842 \\ 3.4111 & -1.6397 & -29.0000 \end{pmatrix}. \tag{39}$$

The characteristic equations of the Jacobian matrix (29) is

$$\lambda_1^3 + 21.79\lambda_1^2 - 312.44\lambda_1 - 2796.9. \tag{40}$$

Solution of (40) results into single positive and two negative eigenvalues:

$$\lambda_{11} = -29.21, \lambda_{12} = -6.75, \lambda_{13} = 14.17. \tag{41}$$

Equation (41) illustrates that two states will move away from E_1, while a single state will move inward towards equilibria: E_1, and such information shows occurrence of the saddle. The Jacobian matrix at E_2 is

$$J|_{E_2} = \begin{pmatrix} -7.0588 & -4.7993 & 5.0421 \\ 15.1078 & 14.2667 & 16.0016 \\ 26.8220 & -22.1560 & -29.0000 \end{pmatrix}. \tag{42}$$

And the corresponding characteristic equation is

$$\lambda_2^3 + 21.79\lambda_2^2 - 17.93\lambda_2 + 7361.79. \tag{43}$$

Solution of (43) gives three eigenvalues with one negative real and two complex numbers with positive real part:

$$\begin{aligned} \lambda_{21} &= -30.37, \\ \lambda_{223} &= 4.2871 \pm 14.9684\iota. \end{aligned} \tag{44}$$

Equation (44) describes occurrence of the unstable spiral. In a similar fashion, one can achieve

$$\begin{aligned} \lambda_{31} &= -30.4682, \\ \lambda_{323} &= 4.3380 \pm 19.4641\iota, \\ \lambda_{41} &= -35.8534, \\ \lambda_{423} &= 7.0306 \pm 17.3188\iota, \\ \lambda_{51} &= -35.8109, \\ \lambda_{523} &= 7.0094 \pm 20.5301\iota. \end{aligned} \tag{45}$$

Eigenvalues of E_3, E_4, and E_5. In view of (45), equilibrium points, $E_{3,4,5}$ are also unstable spirals.

Analytical results (29–35) are explained in Figure 4, which illustrate trajectories of system (4) around their equilibrium points. Five different colors are used for each equilibrium point, which are also highlighted as a legend in Figure 4. It is observed that $E_{2,3,4,5}$ are unstable spirals plotted in green, brown, blue, and black colors, while red color shows the saddle node. In detail, we can see that the red trajectory starts from E_1 and passes through the regions of E_2, E_3, E_4, and E_5 with the passage of time. The trajectory for E_2 shows a spiral emerging from its equilibrium point and is

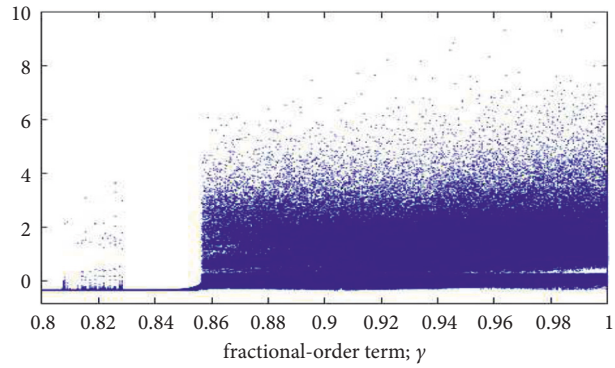

Figure 3: Bifurcation diagram of system (4) with respect to γ.

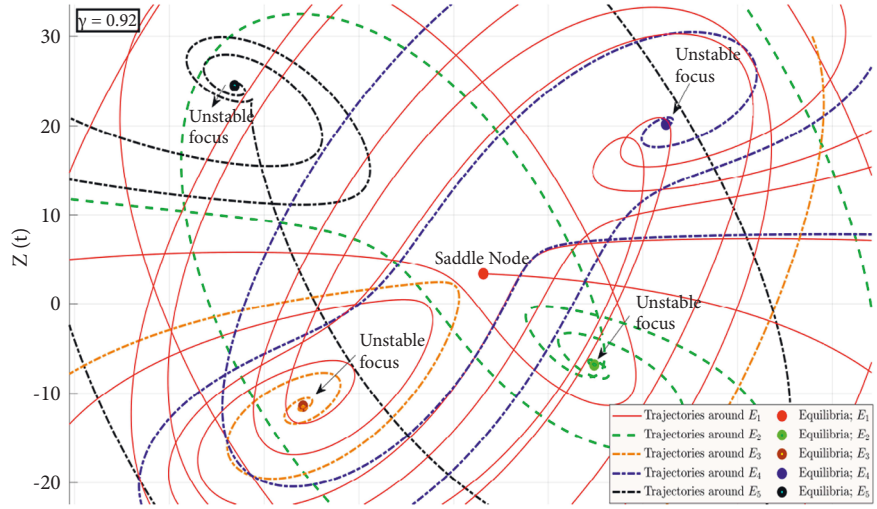

Figure 4: Trajectories of system (4) around equilibrium points.

moving away from it. After some time it has been observed that the green trajectory is acting as a heteroclinic orbit: E_5. The same theory can be observed between E_2 and E_3, when a brown colored orbit starts with high unstable oscillations and approaches to a region occupied by E_2. Apart from these four unstable spirals, one can also locate saddle node equilibria E_1 in the red color, in which its trajectory passes through regions acquired by unstable spirals and act as a separatrix between them. For further analysis, we have extended time for observing the trajectories around five equilibrium points in the greater domain. It has been analyzed that four unstable equilibrium points are self-exciting attractors and occupy four basins. Moreover, the combination of all these four regions leads to the concept of a strange attractor in system (4). Studying in more depth, it has been also observed that the saddle node in the global domain is busy in separating regions of self-exciting attractors. For getting more knowledge about chaoticity in the fractional-order gyrostat system (4), some basic results are used for the possibility and detection of chaos. □

5.1. Lyapunov Exponents. The Lyapunov exponent is one of the fundamental results, which help researchers in pointing out existence of unpredictability in trajectories of their corresponding systems. Moreover, in a three-dimensional autonomous system of ordinary differential equations, there exist three Lyapunov exponents λ_i, $i = 1, 2, 3$. Now, if $(\lambda_1, \lambda_2, \lambda_3) = (+ive, 0, -ive)$, then it shows existence of chaos, whereas $(-ive, -ive, +ive)$ illustrates the existence of periodic solutions. In Figure 5, three Lyapunov exponents can be observed, emerging from $(-9, 11, -30)$ and leading to $(-26.51, 0, 4.87)$, which motivated us to work further on it and find out chaotic trajectories in it. For further investigation, we have used the concept of the bifurcation diagram [12].

5.2. Bifurcation Leading to Chaos. For confirmation of existence of chaos in our proposed model (4), we fixed all other parameter values except for μ_y. For damping coefficient, μ_y, it is observed in Figure 6 that there seems no bifurcation in system (4) for $\mu_y \in (1, 3.6)$. The single bifurcation emerges at $\mu_y = 3.6$ and continues till $\mu_y = 5$, which changes into period doubling bifurcation (**PDB**) for $5 \leq \mu_y \leq 5.2$. Trajectories of our proposed system jump into the chaotic region for μ_y lying in interval $(5.2, 6.5)$. One can observe symmetric behavior in sense of bifurcation leading to chaos in Figure 6. If we start from $\mu_y = 11$, two lines can be observed that are

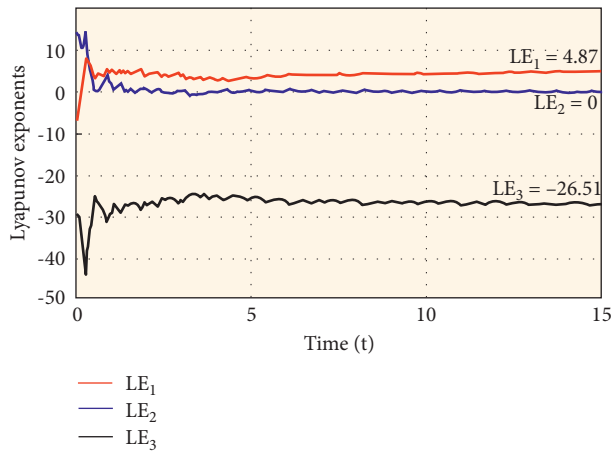

Figure 5: Lyapunov exponents of system (4).

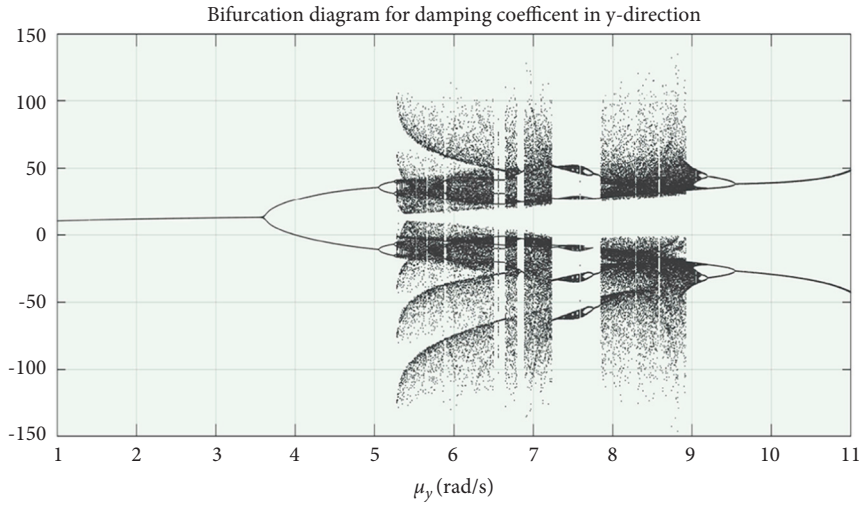

Figure 6: Bifurcation diagram for damping coefficient, μ_y in system (4).

converted into period doubling bifurcations, then period 2 ⟶ period 4 ⟶ 8 ⟶ chaotic region. This concept is also explained with the aid of a series of phase portraits, which confirms chaotic behavior in our proposed system. Therefore, we have divided bifurcation diagram 5 in nine regions and plotted phase portraits to their corresponding values.

Figure 2 is validation of Figure 6, which explains existence of chaos in detail by moving clockwise or anticlockwise. Therefore, we have an indexed sequence of phase portraits for μ_y. If we start from region 1, a spiral trajectory can be observed and is expanding in regions 2 and 3. This trajectory is converted into period doubling and period 4 bifurcations in region 4 and 5 for $\mu_y = 4$ to 5.1, respectively. In region 6, chaotic movement of trajectories can be observed, which gradually declines to period 8 ⟶ period 4 ⟶ period 2 bifurcations by moving in the anticlockwise direction from region 6 to 9. Similarly, if we begin in the clockwise direction, region 9 to 1, one can see trajectory starts with period doubling bifurcation for $\mu_y = 9.6$ is gradually increasing to period 4 ⟶ period 8 ⟶ chaos from region 9 to 6, then decline in a symmetric way is observed from chaos to the period doubling bifurcation till region 4 which finally shrinks into spiral and bifurcation disappearing in region 3 to 1.

Figure 7 is the series of Lyapunov exponents corresponding to each subregion of the bifurcation diagram (plotted in Figure 6). In Figure 2, the existence of chaos in a symmetrical way is thoroughly discussed, but in Figures 7(a)–7(h) the same concept is explained in more detail where for each value of the damping coefficient μ_y; there exist different values of Lyapunov exponents. Moreover, it is also observed that the Lyapunov exponent of system (4) tends to $(-ive, 0, +ive)$ as the damping coefficient μ_y approaches to 6.43.

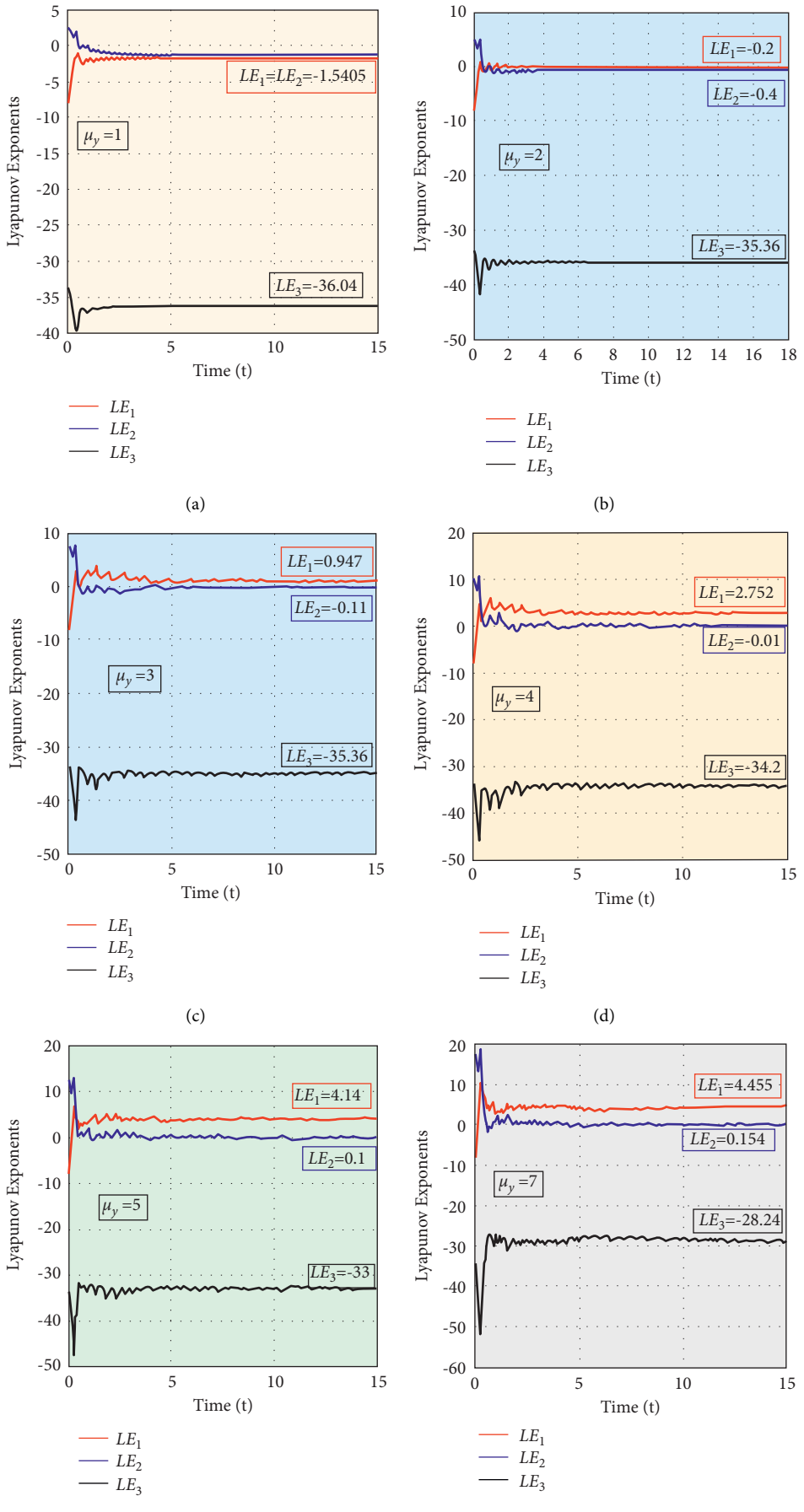

Figure 7: Continued.

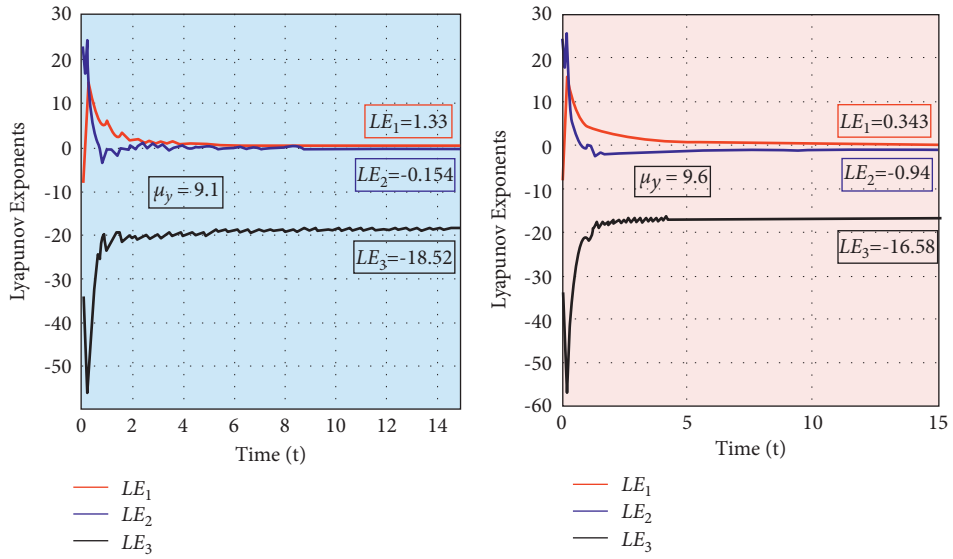

Figure 7: Lyapunov exponents corresponding to each subregion in Figure 6.

6. Conclusion and Future Work

An integer ordered dynamical system of the gyrostat was considered by researchers since decade, and a variety of work related to chaos was achieved with the help of sensitivity in its initial conditions. But we have analyzed the gyrostat model with modification by attaching a rotatory cylinder and conversion into fractional order for the first time. Several theorems were proved in this work for the existence of solution and Ullam–Hyers stability. Moreover, dealing with the fractional-order system does not work on *ODE*45; therefore, an iterative scheme was designed for system (4) to attain chaos in the fractional order. Studying local dynamics of system (4) leads to five solutions with four unstable spirals and one saddle node, but observing trajectories around these equilibrium points in global domain acted as a self-exciting attractor and separatrix. In future, we aim to target fractional-order dynamical systems for codimension 2 bifurcations, which itself is a tedious task due to a large number of involved parameters. Apart from bifurcation, our future aim also involves application of (integer and fractional) ordered chaotic systems in strategy-based mobile gaming.

Appendix

Our discretization scheme is based on an iterative technique; therefore, for $n = 0$ and 1, analytical work is presented in Section 3. But increasing the number of n leads to tedious analytic. Hence, for $n = 2$, the leftover calculation in equation (25) is done here:

$$\begin{cases} \rho_x^1 = \kappa_{x2}(1 - I_x) + (I_y - I_z)\rho_x\rho_{x1} - \rho_x(h_z - h_y) - \mu_x x_0 + \overline{x}\cos(\theta) - \overline{y}\sin(\theta), \\ \rho_x^2 = \mu_x\kappa_{x1} - \dfrac{I_x\mu_x\kappa_{x1}}{\Gamma(\gamma+1)} + \dfrac{\rho_x\kappa_{x1}(I_y - I_z)[(I_x - I_y)y_1 - h_y](h_z + 1)}{(\Gamma(\gamma+1))^2} z^\gamma \\ + \dfrac{\rho_x\kappa_{x1}(I_y - I_z)[(I_z - I_x)z_1 - h_y](h_y + 1)}{(\Gamma(\gamma+1))^2} y^\gamma - \dfrac{\mu_x\kappa_{x2}}{\Gamma(\gamma+1)}, \\ \rho_x^3 = \dfrac{[(I_z - I_x)z_1 - h_y][(I_x - I_y)y_1 - h_y]\kappa_{x1}^2}{(\Gamma(\gamma+1))^4} y^\gamma z^\gamma + \dfrac{\mu_x\kappa_{x1}}{\Gamma(2\gamma+1)}, \end{cases} \tag{A.1}$$

where

$$\begin{aligned}\rho_x &= \frac{\kappa_{y1}\left(1+I_y\right)-\left(I_z-I_x\right)z_1x_0+x_0h_y-\mu_y y_0-\overline{x}\sin\left(\theta\right)-\overline{y}\cos\left(\theta\right)}{\Gamma\left(\gamma+1\right)}y^{\gamma}+y_0+\frac{\kappa_{y1}}{\Gamma\left(2\gamma+1\right)}y^{2\gamma},\\ \rho_{x1} &= \frac{\kappa_{z1}\left(1+I_z\right)-\left(I_x-I_y\right)y_1x_0+x_0h_y-\left(\mu_z-h_y\right)z_0-\overline{z}}{\Gamma\left(\gamma+1\right)}z^{\gamma}+z_0+\frac{\left(\mu_z-h_y\right)\kappa_{z1}}{\Gamma\left(2\gamma+1\right)}z^{2\gamma}.\end{aligned} \tag{A.2}$$

In a similar way, the values of ϱ_y^i are calculated as

$$\begin{cases}\varrho_y^1=\kappa_{y2}\left(1-I_y\right)+\left(I_z-I_x\right)\tilde{\mathrm{n}}_y\tilde{\mathrm{n}}_{y1}-\tilde{\mathrm{n}}_{y1}h_z+\mu_y y_0+\overline{x}\sin\left(\theta\right)+\overline{y}\cos\left(\theta\right),\\ \varrho_y^2=\kappa_{y1}-\frac{\kappa_{y1}}{\Gamma\left(\gamma+1\right)}-\frac{\varrho_y\left[\left(I_y-I_z\right)z_1-h_z\right]\kappa_{y1}}{\left(\Gamma\left(\gamma+1\right)\right)^2}x^{\gamma}-\frac{\mu_y\kappa_{y2}}{\Gamma\left(\gamma+1\right)}-\frac{\varrho_{y1}\left(I_z-I_x\right)\left(I_x-I_y\right)x_1\kappa_{y1}}{\left(\Gamma\left(\gamma+1\right)\right)^2}z^{\gamma},\\ \varrho_y^3=\frac{\left(I_x-I_y\right)\left(I_z-I_y\right)\left[\left(I_y-I_z\right)z_1-h_z\right]\kappa_{y1}}{\left(\Gamma\left(\gamma+1\right)\right)^4}x^{\gamma}y^{\gamma}+\frac{\mu_y\kappa_{y1}}{\Gamma\left(2\gamma+1\right)},\end{cases} \tag{A.3}$$

With

$$\begin{aligned}\varrho_y &= \frac{\kappa_{z1}\left(1+I_z\right)-\left(I_x-I_y\right)x_1y_0+x_1h_y+\left(\mu_z-h_y\right)z_0+\overline{z}}{\Gamma\left(\gamma+1\right)}z^{\gamma}+z_0-\frac{\left(\mu_z-h_y\right)\kappa_{z1}}{\Gamma\left(2\gamma+1\right)}z^{2\gamma},\\ \varrho_{y1} &= \frac{\kappa_{x1}\left(1+I_x\right)-\left(I_y-I_z\right)z_1y_0+y_0h_z-z_1h_y-\mu_x x_0-\overline{x}\cos\left(\theta\right)+\overline{y}\sin\left(\theta\right)}{\Gamma\left(\gamma+1\right)}y^{\gamma}+x_0-\frac{\mu_x\kappa_{x1}}{\Gamma\left(2\gamma+1\right)}x^{2\gamma}.\end{aligned} \tag{A.4}$$

Finally, the values of ς_z^i are

$$\begin{cases}\varsigma_z^1=\kappa_{z2}\left(1-I_z\right)+\left(I_x-I_y\right)C_z\varsigma_{z1}-\varsigma_z-\varsigma_{z1}\left(\mu_z-h_y\right)-\overline{z},\\ \varsigma_z^2=\left(\mu_z-h_y\right)L_z+\frac{\left(\mu_z-h_y\right)I_zL_z}{\Gamma\left(\gamma+1\right)}-\frac{x_1\kappa_{z1}\left(I_z-I_x\right)\left[\varsigma_z\left(I_x-I_y\right)+\left(\mu_z-h_y\right)\right]}{\left(\Gamma\left(\gamma+1\right)\right)^2}y^{\gamma}-\frac{\kappa_{z1}\left(\left(I_y-I_z\right)y_1+h_y\right)\left[\varsigma_{z1}\left(I_x-I_y\right)+h_y\right]}{\left(\Gamma\left(\gamma+1\right)\right)^2}x^{\gamma},\\ \varsigma_z^3=\frac{x_1\kappa_{z1}^2\left(I_x-I_y\right)\left(I_z-I_x\right)\left[\left(I_y-I_z\right)+h_y\right]}{\left(\Gamma\left(\gamma+1\right)\right)^4}x^{\gamma}y^{\gamma},\end{cases} \tag{A.5}$$

where

$$\begin{aligned}\varsigma_z &= \frac{I_x\kappa_{x1}+\mu_x x_0+y_2h_z-\left(\left(I_y-I_z\right)y_1+h_y\right)z_0-\overline{x}\cos\left(\theta\right)+\overline{y}\sin\left(\theta\right)}{\Gamma\left(\gamma+1\right)}x^{\gamma}+x_0-\frac{\mu_x}{\kappa_{x1}}\Gamma\left(2\gamma+1\right)x^{2\gamma},\\ \varsigma_{z1} &= \frac{L_y\left(1+I_y+x_1h_y-\mu_y y_0-\left(I_z-I_x\right)x_1z_0-\overline{x}\sin\left(\theta\right)-\overline{y}\cos\left(\theta\right)\right)}{\Gamma\left(\gamma+1\right)}y^{\gamma}+y_0+\frac{\kappa_{y1}}{\Gamma\left(2\gamma+1\right)}y^{2\gamma}.\end{aligned} \tag{A.6}$$

For further iterations, things were very tedious; therefore, we used MATLAB for further numerical calculations.

Data Availability

MATLAB is used for graphs and tedious calculations in this work, and codes are available upon reasonable request from the corresponding author.

Ethical Approval

This paper does not contain any studies with human participants or animals performed by any of the author.

Conflicts of Interest

All authors declare that they have no conflicts of interest.

Authors' Contributions

All authors contributed equally to the writing of this paper. All authors read and approved the final manuscript. Muhammad Marwan conducted formal analysis, methodology, investigation, and writing of the original draft. Gauhar Ali conducted formal analysis, methodology, and conceptualization. Ramla Khan conducted methodology, software, conceptualization, and writing.

References

[1] J. Guckenheimer and P. Holmes, "Nonlinear oscillations, dynamical systems, and bifurcations of vector fields," *Springer Science & Business Media*, vol. 42, 2013.

[2] Q. Yang and G. Chen, "A chaotic system with one saddle and two stable node-foci," *International Journal of Bifurcation and Chaos*, vol. 18, no. 05, pp. 1393–1414, 2008.

[3] M. Marwan, M. Mehboob, S. Ahmad, and M. Aqeel, "Hopf bifurcation of forced chen system and its stability via adaptive control with arbitrary parameters," *Soft Computing*, vol. 24, no. 6, pp. 4333–4341, 2020.

[4] M. Fiaz, M. Aqeel, M. Marwan, and M. Sabir, "Retardational effect and hopf bifurcations in a new attitude system of quadrotor unmanned aerial vehicle," *International Journal of Bifurcation and Chaos*, vol. 31, no. 09, Article ID 2150127, 2021.

[5] X. Zhang and H. Zhu, "Hopf bifurcation and chaos of a delayed finance system," *Complexity*, vol. 2019, Article ID 6715036, 2019.

[6] K. Zhuang, J. Gao, and D. Liu, "Stability and hopf bifurcation in a three-component planktonic model with spatial diffusion and time delay," *Complexity*, vol. 2019, Article ID 4590915, , 2019.

[7] M. Sabir, S. Ahmad, and M. Marwan, "Hopf bifurcation analysis for liquid-filled gyrostat chaotic system and design of a novel technique to control slosh in spacecrafts," *Open Physics*, vol. 19, no. 1, pp. 539–550, 2021.

[8] M. Fiaz, M. Aqeel, M. Marwan, and M. Sabir, "Integer and fractional order analysis of a 3d system and generalization of synchronization for a class of chaotic systems," *Chaos, Solitons & Fractals*, vol. 155, Article ID 111743, 2022.

[9] Diz-Pita Erika, L. Jaume, M. Otero-Espinar Victoria, and V. Claudia, "The zero-hopf bifurcations in the Kolmogorov systems of degree 3 in r3," *Communications in Nonlinear Science and Numerical Simulation*, vol. 95, Article ID 105621, 2021.

[10] B. Francisco and C. Mereu Ana, "Zero – hopf bifurcation in a 3d jerk system," *Nonlinear Analysis: Real World Applications*, vol. 59, Article ID 103245, 2021.

[11] M. R. Cândido and J. Llibre, "Zero-Hopf bifurcations in 3-dimensional differential systems with no equilibria – hopf bifurcations in 3 – dimensional differential systems with no equilibria," *Mathematics and Computers in Simulation*, vol. 151, pp. 54–76, 2018.

[12] M. Marwan and S. Ahmad, "Bifurcation analysis for energy transport system and its optimal control using parameter self-tuning law," *Soft Computing*, vol. 24, no. 22, Article ID 17221, 2020.

[13] G. Qi, "Energy cycle of brushless dc motor chaotic system," *Applied Mathematical Modelling*, vol. 51, pp. 686–697, 2017.

[14] Y. F. Zhang, M. H. Yao, W. Zhang, and B. C. Wen, "Dynamical modeling and multi-pulse chaotic dynamics of cantilevered pipe conveying pulsating fluid in parametric resonance," *Aerospace Science and Technology*, vol. 68, pp. 441–453, 2017.

[15] Y. Yang and G. Qi, "Comparing mechanical analysis with generalized-competitive-mode analysis for the plasma chaotic system," *Physics Letters A*, vol. 383, no. 4, pp. 318–327, 2019.

[16] M. Sabir, M. Marwan, S. Ahmad, M. Fiaz, and F. Khan, "Observer and descriptor satisfying incremental quadratic constraint for class of chaotic systems and its applications in a quadrotor chaotic system," *Chaos, Solitons & Fractals &*, vol. 137, Article ID 109874, 2020.

[17] M. Marwan, M. Z. Abidin, H. Kalsoom, and M. Han, "Generalized full order observer subject to incremental quadratic constraint (IQC) for a class of fractional order chaotic systems," *Fractal and Fractional*, vol. 6, no. 4, 2022.

[18] J. Iqbal, S. Ahmad, M. Marwan, and M. Shaukat, "Control and numerical analysis for cancer chaotic system," *Archive of Applied Mechanics*, vol. 90, no. 12, pp. 2597–2608, 2020.

[19] A. E. Matouk, "Complex dynamics in susceptible-infected models for covid-19 with multi-drug resistance," *Chaos, Solitons & Fractals*, vol. 140, Article ID 110257, 2020.

[20] D. Nadjette, O. Adel, M. B. Iqbal, and G. Giuseppe, "Chaotic dynamics in a novel covid-19 pandemic model described by commensurate and incommensurate fractional-order derivatives," *Nonlinear Dynamics*, vol. 2021, pp. 1–13, 2021.

[21] L. F. Santos and M. Rui, "Bifurcation of equilibria for general case of gyrostat satellite on a circular orbit," *Aerospace Science and Technology*, vol. 105, Article ID 106058, 2020.

[22] M. Z. Abidin and J. Chen, "Global well-posedness of the generalized rotating magnetohydrodynamics equations in variable exponent Fourier – Besov spaces," *Journal of Applied Analysis & Computation*, vol. 11, no. 3, pp. 1177–1190, 2021.

[23] M. Marwan, S. Ahmad, M. Aqeel, and M. Sabir, "Control analysis of rucklidge chaotic system," *Journal of Dynamic Systems, Measurement, and Control*, vol. 141, no. 4, 2018.

[24] M. Z. Abidin, N. Ullah, and Omer Abdalrhman Omer, "Global well-posedness and analyticity of the primitive equations of geophysics in variable exponent Fourier – Besov spaces," *Symmetry*, vol. 14, no. 1, 2022.

[25] A. M. AbdelAty, M. E. Fouda, and A. M. Eltawil, "On numerical approximations of fractional-order spiking neuron models," *Communications in Nonlinear Science and Numerical Simulation*, vol. 105, Article ID 106078, 2022.

[26] Q. Li, S. Liu, and Y. Chen, "Combination event-triggered adaptive networked synchronization communication for nonlinear uncertain fractional-order chaotic systems,"

Applied Mathematics and Computation, vol. 333, pp. 521–535, 2018.

[27] J. Hadi, Y. Amin, M. Munoz-Pacheco Jesus, K. Sezgin, P. Viet-Thanh, and A. Fawaz, "A new fractional-order hyperchaotic memristor oscillator: dynamic analysis, robust adaptive synchronization, and its application to voice encryption," *Applied Mathematics and Computation*, vol. 383, Article ID 125310, 2020.

[28] R. Garrappa, "Trapezoidal methods for fractional differential equations: theoretical and computational aspects," *Mathematics and Computers in Simulation*, vol. 110, pp. 96–112, 2015.

[29] D. Kai, N. Ford, and D. Freed Alan, "Detailed error analysis for a fractional adams method," *Numerical Algorithms*, vol. 36, pp. 31–52, 2004.

[30] R. Garrappa, "On linear stability of predictor-corrector algorithms for fractional differential equations," *International Journal of Computer Mathematics*, vol. 87, no. 10, pp. 2281–2290, 2010.

[31] M. Zayernouri and A. Matzavinos, "Fractional adams–bashforth/moulton methods: an application to the fractional keller –– segel chemotaxis system," *Journal of Computational Physics*, vol. 317, no. 1–14, 2016.

[32] G. C. Wu and D. Baleanu, "Variational iteration method for fractional calculus – a universal approach by laplace transform," *Advances in Difference Equations*, vol. 18, 2013.

[33] Z. M. Odibat and S. Momani, "Application of variational iteration method to nonlinear differential equations of fractional order," *International Journal of Nonlinear Sciences and Numerical Stimulation*, vol. 7, no. 1, pp. 27–34, 2006.

[34] S. Kumar and V. Gupta, "An application of variational iteration method for solving fuzzy time-fractional diffusion equations," *Neural Computing & Applications*, vol. 33, no. 24, Article ID 17659, 2021.

[35] G. Qi and X. Yang, "Modeling of a chaotic gyrostat system and mechanism analysis of dynamics using force and energy," *Complexity*, vol. 1, no. 13, 2019.

[36] A. Wolf, J. B. Swift, H. L. Swinney, and J. A. Vastano, "Determining lyapunov exponents from a time series," *Physica D: Nonlinear Phenomena*, vol. 16, no. 3, pp. 285–317, 1985.

[37] M. Schmutz and M. Rueff, "Bifurcation schemes of the lorenz model," *Physica D: Nonlinear Phenomena*, vol. 11, no. 1, pp. 167–178, 1984.

[38] H. Bi, G. Qi, and J. Hu, "Modeling and analysis of chaos and bifurcations for the attitude system of a quadrotor unmanned aerial vehicle," *Complexity*, vol. 2019, Article ID 6313925, , 2019.

[39] Anatoliui Aleksandrovich Kilbas, H. M. Srivastava, and J. J. Trujillo, *Theory and applications of fractional differential equations*, Vol. 204, Elsevier, , Amsterdam, 2006.

[40] T. Burton and C. Kirk, "A fixed point theorem of krasnoselskii—schaefer type," *Mathematische Nachrichten*, vol. 189, no. 1, pp. 23–31, 1998.